Eur. Phys. J. E **4**, 489–504 (2001)

THE EUROPEAN PHYSICAL JOURNAL E

EDP Sciences

Small-angle X-ray diffraction study of the thermotropic and lyotropic phases of five alkyl cyclic and acyclic disaccharides: Influence of the linkage between the hydrophilic and hydrophobic moieties

X. Auvray[1,a], C. Petipas[1], C. Dupuy[1], S. Louvet[1], R. Anthore[1], I. Rico-Lattes[2], and A. Lattes[2]

[1] UMR CNRS 6634, Faculté des Sciences et des Techniques L.E.F.G.S., 76821 Mont Saint Aignan Cédex, France
[2] Laboratoire des IMRCP, UMR CNRS 5623, Université Paul Sabatier, 118 route de Narbonne, 31062 Toulouse Cédex, France

Received 31 March 2000

Abstract. We present a comparative study of the thermotropic and lyotropic phases of 5 surfactants with an aliphatic chain of 12 carbon atoms and a cyclic or acyclic sugar head with different linkages between the two moieties. These linkages can concern different chemical groups or different orientations between the head and the chain. The compounds included the α- and β-N dodecyl-D-maltosides, N-dodecylamino-1-deoxylactitol, N-dodecyl lactobionamide and N-acetyl N-dodecyl lactosylamine. The influence of the polar head (with closed- and opened-type sugars) and the linkage with the hydrocarbon chain on the phases obtained by the heating of the anhydrous compounds and after addition of water was studied by X-ray diffraction and optical microscopy. In the anhydrous state, the surfactants were either crystalline or amorphous. On heating, they went through a liquid crystal smectic phase which, in some cases, was preceded by solid-to-solid transitions. On addition of water, the sequence of phases from the micellar phase to the lamellar phase was accounted for in terms of the geometric model of Sadoc and Charvolin. However, with certain surfactants this sequence was not complete, and the domains of existence of phases were altered.

PACS. 61.30.Eb Experimental determination of smactic, nematic, cholesteric and other structures – 61.10.Nz Single crystal and powder diffraction – 64.70.Md Transitions in liquid crystals

1 Introduction

Surfactants derived from sugars represent an interesting class of amphiphiles that are biodegradable, biocompatible and can be synthesized from sustainable agricultural products [1]. In view of their highly specific properties, they have been used as replacements for conventional surfactants in the extraction, purification and crystallization of membrane proteins [2], and are also used as emulsifying agents [3] and in cosmetic formulations. They are now produced on an industrial scale [4]. The non-ionic surfactant properties of the alkylglucosides and alkylpolyglucosides can be compared with those of the n-alkylpolyethylene glycol ethers (C_nEO_m) or other surfactants [5, 6]. Functional groups may be linked to the sugar moiety [7–9] producing surfactants with highly specific properties. The sugar-based derivatives, which can be produced in a number of molecules, are more complex than conventional surfactants: the effects of oligosaccharide stereochemistry on the physical properties of aqueous synthetic glycolipids have been the subject of study over recent years [10].

The sugar-based derivatives are composed of three main parts:

– a hydrophilic head consisting of cyclic or acyclic sugar residues based on one or more rings of 5 or 4 carbons bearing different functional groups [9–12];

– a hydrophobic part;

– a linkage between the two parts: an oxygen or sulphur atom [13], a group with various degrees of ionization or polarizability [14, 15]. The head and the chain may also be in either the α or β orientation [16].

To demonstrate the influence of the linkage upon association with water and the formation of liquid crystal phases as a function of surfactant concentration, we studied five surfactants with a chain length of 12 carbon atoms and with polar heads consisting of two sugar residues: i) N-dodecylamino 1 deoxylactitol (L) (Fig. 1a), where the sugar head is linked to the hydrocarbon chain by the hydrophilic, basic and partially ionized, amino linkage NH. ii) N-dodecyl lactobionamide (B) (Fig. 1b) where the acyclic sugar residue is linked to the hydrophobic chain by an amide linkage (-C-O-NH-). The amide group forms strong intramolecular hydrogen bonds and also has a dipolar moment [14]. iii) N-acetyl-N-dodecyl

[a] e-mail: xavier.auvray@univ-rouen.fr

Table 1. Volume of surfactant molecules. V_m: molecular volume. V_h: polar head volume. Chain volume = 0.354 nm^3. V_h/V_m: the ratio of the volume of the polar head to the overall volume of the molecule is listed for comparison with other reports.

Product	α Maltoside (αM)	β Maltoside (βM)	Lactitol (L)	Bionamide (B)	Acetyl (Ac)
V_m (nm^3)	0.691	0.691	0.681	0.708	0.750
V_h (nm^3)	0.337	0.337	0.327	0.354	0.396
V_h/V_m	0.49	0.49	0.48	0.50	0.53

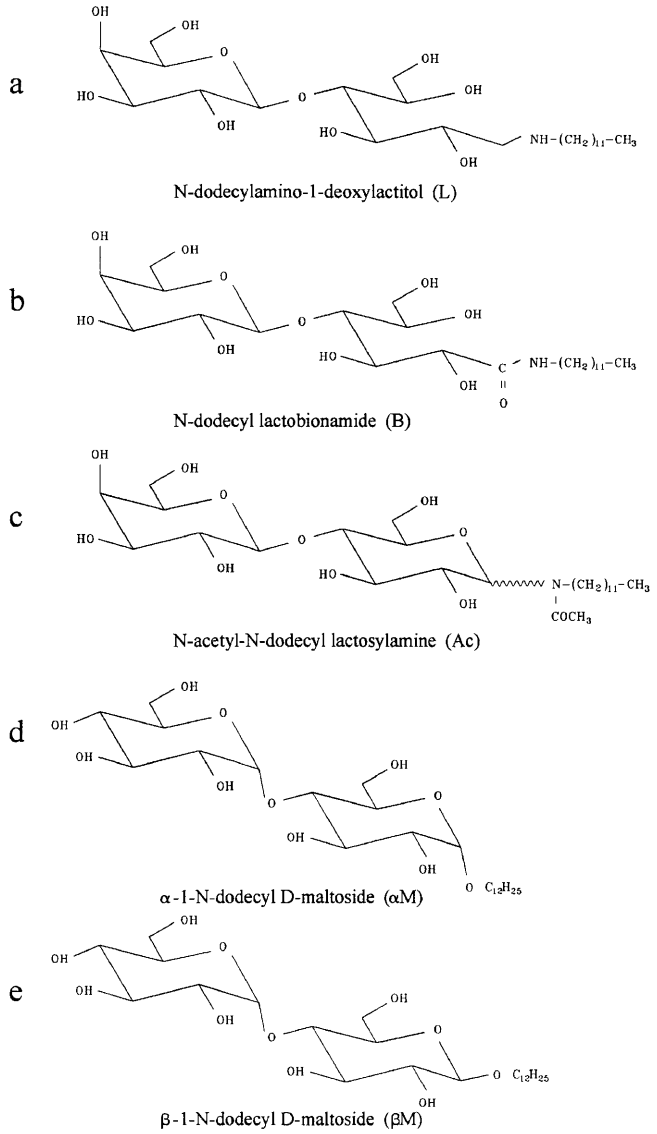

Fig. 1. Chemical structure of the five surfactants: a) (N-dodecylamino)-1-deoxylactitol; (L). b) (N-dodecyl) lactobionamide; (B). c) (N-acetyl N-dodecyl) lactosylamine; (Ac). The squiggly line between the N atom and the sugar ring denotes that the compound is a mixture of alpha and beta anomers. d) α-1-N-dodecyl D-maltoside; (αM). e) β-1-N-dodecyl D-maltoside; (βM).

lactosylamine (Ac) (Fig. 1c) where the two sugar residues and the chain are linked with a bulky (N-CO-CH_3) group, which also has a hydrophobic group [15]. iv) α- and β-1 N dodecyl-D-maltosides (αM) or (βM) (Fig. 1 d and e) where the linkage between the chain and the head is either α or β type.

The binary phase diagrams of (L) and (βM) in water have been reported elsewhere [12] in a study of the influence of chain length on the lyotropic liquid crystal phases. We have included these phase diagrams in the present publication. The study of the micellization of all these compounds by X-ray and neutron scattering has previously been published [16–18]. Two types of micelles were observed in the concentration domain C = c-(c.m.c.) of 0.02 mole l^{-1} to 0.1 mole l^{-1}: i) The micelles of (Ac) and (αM) were quasi-spherical, the aggregation numbers and the core radii are 64 and 75, 1.75 nm and 1.86 nm respectively. ii) The micelles of (L), (B), (βM) were of anisotropic form; the aggregation numbers are 88, 95 and 132, respectively.

The phase diagrams were investigated by optical microscopy and by small- and wide-angle X-ray diffraction. (The terms "small- and wide-angle X-ray diffraction" are defined in the experimental section). The structures and parameters of the ordered phases could be determined using these techniques.

We also characterized the anhydrous compounds and their transition temperature by X-ray diffraction and optical microscopy. The molecules of the five compounds behave amphotropically; they exhibit thermotropic and lyotropic mesophases.

2 Experimental

2.1 Preparation of compounds

The synthesis of (N dodecylamino) lactitol is described elsewhere [2d], [19] as is (N-acetyl N-dodecyl) lactosylamine [15]. The α- and β-1 N dodecyl-D-maltosides (98%) were supplied by Aldrich and used without further purification.

2.2 Physico-chemical characteristics

The volume V_m of surfactant molecules was obtained from density measurements of surfactant solutions in a previous study [16–18]. The values of V_m are listed in Table 1 along with the volumes of the different polar heads V_h of each compound. The volume of the alkyl chain V_{ch} is 0.354 nm^3 [20]. These values are used to calculate the volume fraction C_v of the sample from the weight fraction C_m of the sample (surfactant/(surfactant + water)). The

volume fraction allows the calculation of the aggregation number N and the dimensions of the aliphatic cores of the micelles.

With M_t the molecular weight of the surfactant, M_s the molecular weight of the solvent and V_s the volume of a molecule of solvent:

$$C_v = (V_m/M_t)/(V_m/M_t + (V_s/M_s)(1/C_m - 1)), \quad (1)$$

The volume fraction of the apolar moiety is given by

$$C_{v,ch} = C_v V_{ch}/V_m. \quad (2)$$

2.3 X-ray diffraction

The X-ray diffraction study was carried out by use of a small-angle diffraction set-up with a linear position-sensitive detector. The Cu-$K\alpha_1$ radiation ($\lambda = 0.154$ nm) monochromatized by a bent quartz crystal is focused at the detector. The detector is placed 24.1 cm away from the sample. With this geometry, the range of scattering vectors $\mathbf{s}$ is

$$5 \times 10^{-2}\,\mathrm{nm}^{-1} < s < 1.2\,\mathrm{nm}^{-1}\,,$$

with $s = 2\theta/\lambda, 2\theta$ being the angle between incident and scattered beams. This scattering vector range corresponds to the following d-spacing range:

$$20.0\,\mathrm{nm} > d > 0.83\,\mathrm{nm}\,.$$

The height of the X-ray beam on the sample was set at 1.5 mm. A system of moving horizontal slits in front of the detector reduced the effects of beam height; they were adjusted to form a horizontal entrance slit of around 3 mm.

The sample cell was made of brass and sealed with flat Mylar windows. The sample thickness was set at 1 mm with a Teflon spacer. To check homogeneity and to observe the effects of texture and the possible formation of large liquid crystals, the sample could be moved in the horizontal and vertical axes over an area of 25 mm^2. As the cell rotates around its vertical axis, it is possible to check that the observed intensity of diffraction rings is not due to partial orientation of the samples or to the growth of some crystallites. The sample was heated from 5 to 95 °C by circulation of water. The temperature of the water bath was regulated to ±0.1 °C.

A conventional X-ray diffraction apparatus was also used with a focused beam and a camera. In this case, the range of scattering vectors was

$$1.0\,\mathrm{nm}^{-1} < s < 5\,\mathrm{nm}^{-1}\,,$$

corresponding to the d spacing range:

$$1\,\mathrm{nm} > d > 0.2\,\mathrm{nm}\,.$$

In this case, the patterns are obtained at room temperature and the method is called wide-angle diffraction. This enables the alkyl chains state to be observed.

2.4 Sample preparation

The weight fraction of surfactant C_m in each sample ranged from 0.4 to 0.95. The required amounts of surfactant and water were weighed and mixed. The sample holder containing approximately 40 mg of product was weighed before and after the X-ray study. When different samples were prepared at more than 2% surfactant intervals the systematic decrease of the phase parameter with the composition could be observed. Thus, the uncertainty in the composition of the sample ($\Delta C_m/C_m$) was estimated to be less than 1%. To study the lyotropic phase behaviour of each compound, a number of X-ray diffraction patterns were recorded over 1800 s at the same temperature to ensure equilibrium conditions and to control the evaporation which produces a shift of Bragg peaks due to the parameter change or a phase transformation.

2.5 Optical microscopy

The microscopic examinations were carried out using a Jenapol polarizing microscope fitted with a Mettler hot plate. The phases were observed by a water penetration method. Both the hexagonal and lamellar phases are birefringent and exhibit characteristic textures, whereas the cubic phases are optically isotropic and black. A micellar phase and a cubic phase can be distinguished by their viscosity.

3 Phase characterization of compounds

The liquid crystalline transition temperatures T_f determined by thermal optical microscopy are listed in Table 2. The accuracy of the determinations of T_f depends on the fluidity of the liquid crystal. Except for the highly fluid (βM) at 103 °C, the formation of characteristic textures such as oily streaks or fan textures spread over about 4-5 °C with a temperature rise of 3 °C per minute. At temperatures of about 150 °C, the compounds darkened and decomposed rapidly, which prevented determination of the clarification point and all determinations *in situ* using conventional methods. The smectic phase was supercooled to room temperature; it remained unchanged and was studied at 20 °C.

The X-ray diffraction study indicated the existence of quite different solid states between compounds (αM), (βM) and (B) and compounds (L) and (Ac). The diffraction pattern of the first three compounds consisted of fine lines that are characteristic of crystalline solids in both small and wide angles (d reticular spacings for small angles are given in Tab. 2), while the patterns of the latter two compounds consisted of rings in both small and wide angles (Tab. 2). At room temperature, the crystal structure of (αM), (βM) and (B) was of lamellar type and the layer spacing d was deduced from the position of the first intense line, which was the same for (αM) and (βM)

Table 2. Liquid crystalline transition temperatures and X-ray diffraction diagrams. T_f: temperatures of chain melting. T: temperature at which spectra were recorded *in situ*. T correponds to the initial temperature (20 °C) or a temperature slightly above the solid/solid transformation. d: lattice spacings. d^*: spacings corresponding to the scattering ring positions.

Compound	α Maltoside (αM)		β Maltoside (βM)		Bionamide (B)	Acetyl (Ac)	Lactitol (L)
T_f °C	128		103		140	120	120
T °C	20	50	20	80	20	20	20
	3.35	3.245	3.35	4.15	3.175	3.45*	4.44*
Diffraction	1.675	1.615	1.95	2.075	1.585		
pattern	1.12	1.065	1.66	1.572	1.055	0.42*	0.42*
d (nm)	0.995		1.23	1.36			
d^* (nm)			1.17	1.235			
			1.10	1.19			
			0.990	1.12			

(3.35 nm) and slightly lower (3.17 nm) for (B). These spacings probably correspond to fully extended interdigitated chains or partially interdigitated polar heads.

The diffraction patterns of the compounds and their evolution on heating were different.

3.1 Compound (B)

At 20 °C, the diffraction lines corresponded to orders 1, 2 and 3 of the lamellar crystals. No solid/solid transition was detected up to 140 °C. This higher transition temperature was attributed to the presence of the amide group conferring strong cohesion between polar heads. In the supercooled smectic phase (from 145 °C) the interlamellar spacing was 4.02 nm. Second- and third-order diffraction lines were also observed. The increase of interlamellar spacing on melting of the chains was consistent with a model of rigid interdigitated chains in the lamellar crystal.

3.2 Compound (αM)

A fourth line (0.995 nm) was noted along with the 3 lines (orders 1, 2 and 3), and was attributed to the order of the polar heads. A solid/solid transition was observed around 50 °C, which corresponded to a smaller interlamellar spacing (from 3.35 nm to 3.24 nm) thought to be due to a weak modification of the interdigitation of the molecules. This transformation was reversible and the diffraction pattern, after cooling, was identical to the initial one.

3.3 Compound (βM)

The diffraction pattern of this compound was more complex with additional lines observed at small angles. The powder pattern at small and wide angles was altered around 70 °C with a solid/solid transformation and the interlamellar spacing increased from 3.35 nm to 4.15 nm. On cooling, the crystal only returned to its initial state after being left for around a week at 20 °C. The intermediate patterns were highly complex. The marked increase (3.35 nm to 4.15 nm) of the interlamellar spacing can be explained by the disconnecting of the extended chains. The β configuration favours mobility of the polar head relative to the chain/head interface. The presence between 80 °C and 103 °C (T_f) of disconnected rigid chains can account for the low value of T_f compared to the other compounds and the discontinuity of the viscosity. (Marcus [21a] and Pfannemuller [21b] found the same melting point). This is because the interaction between disconnected alkyl chains is smaller than between interdigitated alkyl chains ($T_f = 128$ °C for (αM)). The solid phase with a large parameter was only stable at a high temperature. On cooling, the lattice with a parameter close to the bilayer spacing of the smectic phase is deformed, giving rise to wide diffuse lines and intermediate patterns. Recrystallization to the initial state thus takes time.

3.4 Compounds (L) and (Ac)

In the solid state, (L) and (Ac) are not crystallized. The first scattering ring at a small angle is characteristic of the absence of a long-range order. The second ring at $s = 2.38\,\mathrm{nm}^{-1}$ (0.42 nm) is characteristic of a gel phase. It is very probable that the amorphous state arises from the liquid surfactant which consists of separated polar and apolar regions depending on the alkyl chain length. The spacings d^* (3.85 nm and 4.44 nm, respectively) were calculated from the positions of the maximum intensity of the scattering rings and are characteristic of spacing between polar head clusters (Tab. 2). According to a previous study the increase of d^* is 0.6 nm for each additional (-CH_2-CH_2-) group in the chain of the N-alkylamino-1-dioxylactitol [12]. Theoretically, by addition of two CH_2 the extended chain length increases to 0.25 nm [20].

On heating, these two compounds do not crystallize; around 120 °C, the polar heads self-assemble to form bilayers while the chains become more fluid through a transformation which occurs gradually. A supercooled smectic phase can be obtained. The interlamellar spacing of the liquid crystal obtained with (Ac) was equal to that of the liquid crystal of (B) measured under the same conditions.

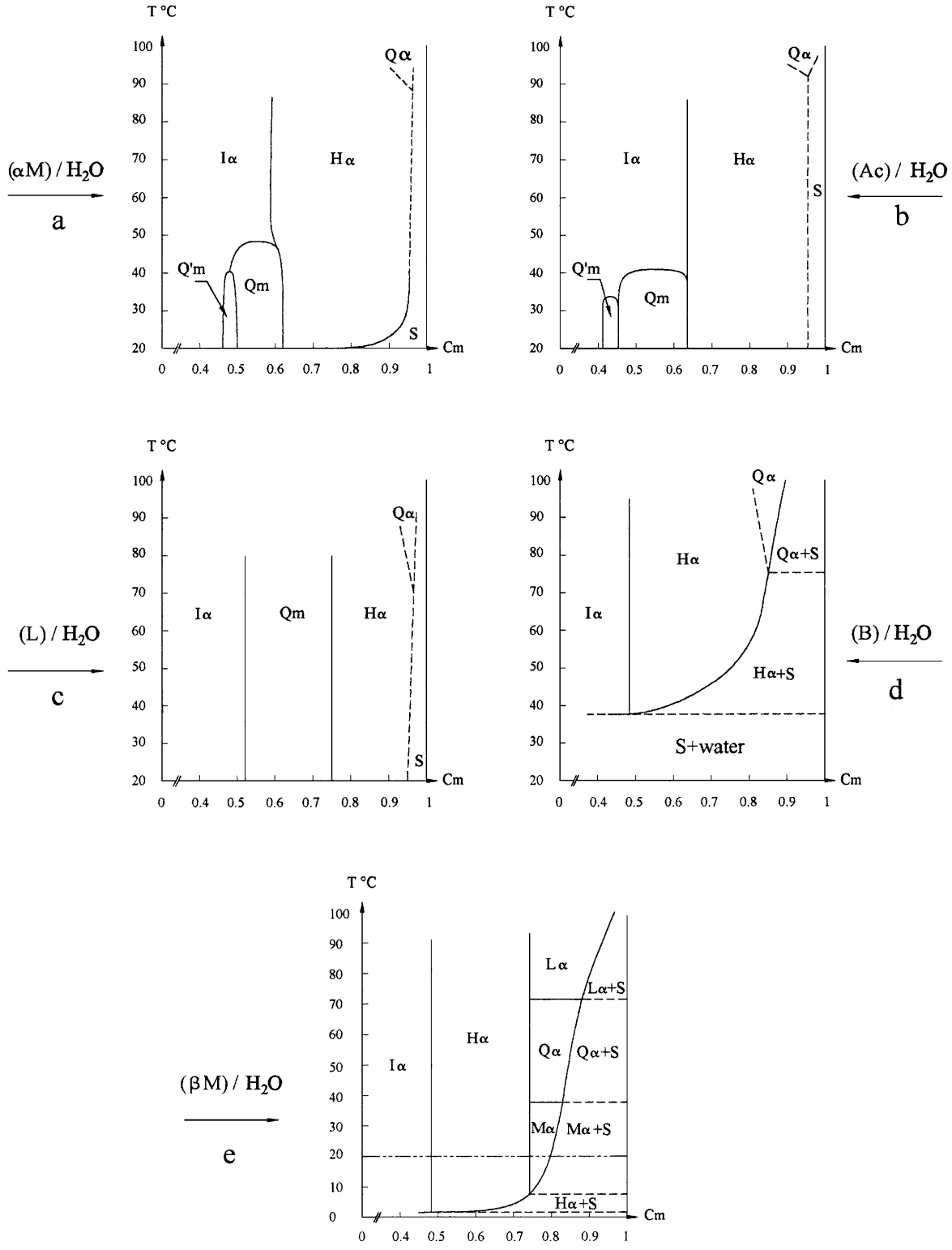

Fig. 2. Binary phase diagrams. a) α-1-N-dodecyl D-maltoside/water. b) (N-acetyl N-dodecyl) lactosylamine/water. c) (N-dodecylamino)-1-deoxylactitol/water. according to reference [12]. d) (N-dodecyl) lactobionamide/water. e) β-1-N-dodecyl D-maltoside/water according to reference [12]. Symbols: $I\alpha$: micellar phase. S: hydrated solid compound. The other symbols are defined in the text.

Table 3. Cubic phases Q'_{m} and Q_{m} in the (αM)/water system. d_{hkl}: reticular spacings corresponding to spectra obtained with the ordered micellar cubic phase (Im3m) Q'_{m} at 10 °C for a weight fraction of surfactant $C_{\mathrm{m}} = 0.44$, and the ordered micellar cubic phase (Pm3n) Q_{m} at 20 °C for a weight fraction $C_{\mathrm{m}} = 0.62$. The lines at 2.43 and 2.18 nm are broad and can be interpreted as a set of unresolved lines formed by (400, 411) and (420, 421 and 422), respectively. $a_{Q'\mathrm{m}}$ and $a_{Q\mathrm{m}}$ are the lattice parameters of both phases Q'_{m} and Q_{m}, respectively.

Q'_{m} $a_{Q'\mathrm{m}} = 6.4$ nm		Q_{m} $a_{Q\mathrm{m}} = 10.0$ nm		$h^2 + k^2 + l^2$
d_{hkl} (nm)	hkl	d_{hkl} (nm)	hkl	
		7.07	110	2
		5.00	200	4
4.53	110	4.47	210	5
		4.08	211	6
		3.53	220	8
3.2	200	3.16	310	10
		2.89	222	12
		2.77	320	13
2.62	211	2.67	321	14
		2.43	400,411	16,18
2.27	220	2.18	420,421,332	20,21,22

4 Phase diagrams

The five phase diagrams (T, C_{m}) are given in Figure 2(a, b, c, d and e). The temperature ranged from 20 °C to 95 °C except for the (βM)/water system in which the temperature range extended down to 0 °C (Fig. 2e). On these diagrams the two phase regions are very narrow (in a composition range < 1%) and it has not been possible to determine both boundary concentrations at small miscibility gaps.

All the phases were direct phases and are denoted as follows: i) Q_{m} and Q'_{m} for the micellar cubic phases whose reticular spacings are listed in Table 3 and for which the structural study is discussed below. ii) H_α for the hexagonal phase (space group p6m), determined from the sequence of lines in the following ratios: $1, \sqrt{3}, \sqrt{4}, \sqrt{7}, \sqrt{9}, \sqrt{12}$ and the characteristic textures observed through a polarizing microscope. iii) M_α for the centred rectangular phase (space group cmm) considered as a deformation of the hexagonal phase. This change in symmetry was observed more readily from the diffraction pattern than from the change in microscopic texture. iv) Q_α for the bicontinuous cubic phase (space group Ia3d) determined from the sequence of diffraction lines in the following ratios: $\sqrt{6}, \sqrt{8}, \sqrt{14}, \sqrt{16}, \sqrt{20}, \sqrt{22}, \sqrt{24}$ [11]. v) L_α for the lamellar phase determined from the diffraction lines in the following ratios: 1, 2, and its characteristic textures (focal conic and oily streaks).

For each compound, the parameters of H_α are listed in Table 4 for the volume fraction of the chains at the appearance and disappearance of this phase with increasing surfactant concentration. The Q_α phase has a narrow region of existence in both concentration and temperature. For each compound its lattice parameter is given in Table 4.

4.1 α-1-N-dodecyl maltoside/water diagram (Fig. 2a)

This phase diagram is characterized by the presence of two ordered micellar phases Q'_{m} and Q_{m}, a hexagonal phase H_α and a bicontinuous cubic phase Q_α.

The two ordered micellar phases were observed by polarizing microscopy at 20 °C and on heating the sample. When the water penetrated the crystals of (αM) at 20 °C, two isotropic viscous phases formed between the hexagonal phase and the fluid micellar phase: i) the bubbles of air trapped in both phases (Q_{m} and Q'_{m}) were settled and had faceted boundaries, particularly in the Q_{m} phase. ii) the dark discontinuity of the interfaces enabled observation of these two phases. Observation of the disappearance of these interfaces when the temperature rose, defined their existence region in the diagram.

The existence range of the viscous phase Q'_{m} adjacent to the micellar phase was narrow in both concentration ($0.45 < C_{\mathrm{m}} < 0.52$ at 20 °C) and temperature (20 °C < T < 40 °C). It was identified with some difficulty using the isoplethal method by X-ray diffraction (Tabs. 3 and 5). Its disappearance around 40 °C was determined by optical microscopy.

The second micellar cubic phase existed over a much wider composition range ($0.52 < C_{\mathrm{m}} < 0.62$). Numerous diffraction peaks were observed at 20 °C ($C_{\mathrm{m}} = 0.62$) and were typical of the Pm3n structure with the diffraction lines in the following ratios: $\sqrt{2}, \sqrt{4}, \sqrt{5}, \sqrt{6}, \sqrt{8}, \sqrt{10}, \sqrt{12}, \sqrt{13}, \sqrt{14}$, with a lattice parameter of 10.0 nm (Tabs. 3 and 6). Its disappearance with increasing temperature was observed around 48 °C, both by optical microscopy and X-ray diffraction. For weight fractions around 0.58 and at 48 °C, the pattern of Q_{m} exhibited a micellar scattering; for fractions around 0.62 and at 45 °C, a hexagonal phase pattern was observed with the d_{10} spacing of the hexagonal phase equal to the d_{211} spacing of the cubic Pm3n phase.

The phase H_α was stable over a wider range of composition: $0.62 < C_{\mathrm{m}} < 0.95$.

The phase Q_α with a lattice parameter $a_{Q_\alpha} = 8.51$ nm ($C_{\mathrm{m}} = 0.95$) had a very narrow range and a thermotropic behaviour. It was observed at 90 °C.

4.2 N-acetyl-N-dodecyl lactosylamine/water diagram (Fig. 2b)

This diagram is similar to the (αM)/water diagram with: i) two ordered micellar phases Q'_{m} and Q_{m}. The lattice parameter of Q'_{m} (centred cubic) was 6.6 nm (at $C_{\mathrm{m}} = 0.42$) (Tab. 5), while the characteristics of Q_{m} were observed over a larger concentration range ($0.45 < C_{\mathrm{m}} < 0.63$) and are listed in Table 6. ii) An H_α phase formed as with (αM) from the Pm3n up to a C_{m} of 0.95. iii) A Q_α phase with thermotropic properties and a lattice parameter of 9.3 nm ($C_{\mathrm{m}} = 0.93$) at 95 °C.

Table 4. Hexagonal phase H_α and cubic phase Q_α. $C_{v,ch}$: volume fraction of chains. $Ci_{v,ch}$ and $Cf_{v,ch}$: values of $C_{v,ch}$ at appearance and disappearance of the relevant phases. a_{H_α} and a_{Q_α}: lattice parameters of the H_α and Q_α phases. σ_{H_α} and σ_{Q_α}: areas per polar head of the rods. R_{H_α} and R_{Q_α}: radii of the aliphatic core of the rods.

Compound	H_α					Q_α			
	$C_{v,ch}$		a_{H_α} (nm)	R_{H_α} (nm)	σ_{H_α} (nm^2)	$C_{v,ch}$	a_{Q_α} (nm)	R_{Q_α} (nm)	σ_{Q_α} (nm^2)
(αM)	$Ci_{v,ch}$	0.28	4.61	1.30	0.54	0.49	8.51	1.31	0.47
	$Cf_{v,ch}$	0.48	4.20	1.55	0.46				
(Ac)	$Ci_{v,ch}$	0.27	4.83	1.32	0.54	0.45	9.30	1.35	0.46
	$Cf_{v,ch}$	0.44	4.30	1.50	0.47				
(L)	$Ci_{v,ch}$	0.36	4.53	1.43	0.49	0.49	9.72	1.49	0.41
	$Cf_{v,ch}$	0.48	4.42	1.61	0.44				
(B)	$Ci_{v,ch}$	0.24	6.12	1.44	0.49	0.40	10.75	1.46	0.43
	$Cf_{v,ch}$	0.41	5.10	1.69	0.42				
(βM)	$Ci_{v,ch}$	0.23	5.63	1.42	0.50	0.41	10.34	1.31	0.48
	$Cf_{v,ch}$	0.35	4.86	1.52	0.47				

Table 5. Dimensions of the aggregates in the the micellar phase I_α and the cubic phase Q'_m (Im3m). $C_{v,ch}$: volume fraction of the chains. N: aggregation number. R_{ch}: radii of micelle aliphatic cores assumed to be spherical. $a_{Q'_m}$: cubic lattice parameter. R_s: radii of closely packed micelles.

Phase	Micelles (I_α)			Q'_m (Im3m)				
Parameters	$C_{v,ch}$ 10^{-3}	N	R_{ch} (nm)	$C_{v,ch}$ (nm)	$a_{Q'_m}$ (nm)	N	R_{ch} (nm)	R_s (nm)
(αM)	0.43	72	1.83	0.190	6.4	70	1.81	2.77
(Ac)	0.43	65	1.76	0.160	6.6	65	1.76	2.86

Table 6. Dimensions of the aggregates in the cubic phase Q_m (Pm3n). N: aggregation number. $C_{v,ch}$: volume fraction of the chains, a_{Q_m} cubic lattice parameter, N_a and N_c: aggregation numbers of micelles in Wyckoff positions "a" and "c". Indices i and f are used at onset of Q_m and at the $Q_m \Leftrightarrow H_\alpha$ transition, respectively. R_{ch}: radii of micelle aliphatic cores assumed to be spherical. a_{ch} and b_{ch}: major and minor axes of the aliphatic cores of micelles assumed to be oblate.

Phase	I_α	Q_m (Pm3n)													
Parameters	N	$Ci_{v,ch}$	a_{Q_m},i (nm)	Ni_a	R_{ch} (nm)	Ni_c	a_{ch} (nm)	b_{ch}	$Cf_{v,ch}$	a_{Q_m},f (nm)	Nf_a	R_{ch} (nm)	Nf_c	a_{ch} (nm)	b_{ch} (nm)
(αM)	69	0.230	10.4	66	1.77	99	2.32	1.53	0.280	10.0	72	1.82	108	2.40	1.58
(Ac)	65	0.180	10.9	60	1.72	90	2.25	1.48	0.275	10.5	82	1.90	123	2.51	1.65
(L)	88	0.245	11.0	84	1.92	126	2.52	1.66	0.365	9.9	91	1.99	137	2.59	1.71

4.3 N-dodecylamino 1 deoxylactitol/water diagram (Fig. 2c)

The phase diagram has been published elsewhere [12] and is characterized by: i) A single-ordered phase Q_m with an extended range in both temperature and concentration ($0.52 < C_m < 0.75$). ii) In common with the previous two systems, an H_α phase up to $C_m = 0.95$. iii). A Q_α phase which was observed at 70 °C ($a_{Q_\alpha} = 9.75$ nm at $C_m = 0.95$) over a narrow range of concentration.

4.4 N-dodecyl 1 lactobionamide/water diagram (Fig. 2d)

The Krafft temperature of this surfactant is around 38 °C and the Krafft line exhibited a marked curvature after the appearance of the H_α phase. i) No ordered micellar phase was observed. ii) The H_α phase occurs at 38 °C (0.48). It was in equilibrium with the crystal up to 75 °C ($C_m = 0.85$). It has a lattice parameter of 10.75 nm at 95 °C with $C_m = 0.85$. iii) The Q_α phase appears around 75 °C in equilibrium with the crystal ($C_m = 0.85$), with a lattice parameter of 10.75 nm at 95 °C with C_m close to 0.85.

In these four binary diagrams no L_α phase was observed below 95 °C.

4.5 β-1 N dodecyl-D-maltoside/water diagram (Fig. 2e)

The phase diagram studied over a range of 5 °C to 95 °C has been published elsewhere [12]. In Figure 2e the line at 20 °C was traced to facilitate the comparison with the

other diagrams starting at 20 °C. The diagram of this system was quite different from the previous ones and was characterized by: i) A narrower region of existence of the H_α phase ($0.48 < C_\mathrm{m} < 0.74$). ii) Formation of a centered rectangular phase M_α ($0.75 < C_\mathrm{m} < 0.83$). iii) A wider range of existence of the Q_α phase in both temperature and concentration than in the four previous systems, with a lattice parameter of 10.3 nm at 40 °C with $C_\mathrm{m} = 0.84$. H_α, M_α and Q_α are missing in different reports of the diagram for the (βM)/water system [22]. iv) Presence of an L_α phase with a parameter of 3.92 nm above 75 °C which is close to the temperature of solid/solid transformation of the crystal in the absence of water (Tab. 2).

Along the Krafft line, the transitions $M_\alpha \leftrightarrow Q_\alpha \leftrightarrow L_\alpha$ were observed over a narrow composition range ($0.75 < C_\mathrm{m} < 0.9$), because of the slope of the Krafft line these phases exhibited a marked thermotropic behaviour.

5 Analysis of the phases

For the transitions of phases, the pertinent parameter introduced by Israelachvili [23] is the packing parameter $p = V_\mathrm{ch}/(l.\sigma)$ where σ is an area per polar head at the aliphatic/hydrophilic interface and l the length of the chain. This parameter is $\leqslant 1/3$ for spherical micelles, 1/2 in the hexagonal phase and 1 in the lamellar phase. When the micelles have a local varying curvature the value of p can be calculated at any point from the following relationship [24]:

$$p = 1 - (1/2)(1/R_1 + 1/R_2)l + (1/3)(1/(R_1R_2))l^2\,, \quad (3)$$

$1/2(1/R_1 + 1/R_2)$ is the mean curvature and $1/(R_1R_2)$ is the Gaussian curvature.

The geometric model of Sadoc and Charvolin predicts the following sequence of phases:

$$L_\alpha \leftrightarrow Q_\alpha \leftrightarrow H_\alpha \leftrightarrow Q_\mathrm{m} \leftrightarrow I_\alpha \quad (\text{micelles})\,,$$

with a possibility of deformation of the hexagonal phase [25].

5.1 Cubic micellar phases: Q'_m(Im3m) and Q_m(Pm3n)

5.1.1 Q'_m phase

The X-ray diffraction pattern with only four lines does not allow us to determine a simple or centered cubic structure. The following considerations enable one of the two structures to be eliminated: i) The aggregation number N, determined from the lattice parameter a, the volume fraction of the chains $C_\mathrm{v,ch}$ and the volume of an aliphatic core V_par:

$$N = V_\mathrm{par}/V_\mathrm{ch} = a^3 C_\mathrm{v,ch}/V_\mathrm{ch}, \quad (4)$$

is equal to 45 for (αM) in the case of a simple cubic structure. This aggregation number is lower than that of micelles at low concentration ($N = 69$) and this result is inconsistent with the micelle size increase *versus* the surfactant concentration. Moreover, a cubic stacking of one micelle per unit cell is not stable. The same calculation with a body-centered cubic packing with two micelles per unit cell gives an aggregation number N of 70, which is identical to that for the micelles of (αM) in a diluted solution. A similar result was obtained for (Ac): $N = 65$ for the spherical micelles of the micellar phase at low concentrations above the c.m.c., and $N = 64$ for ordered spherical micelles of the Q'_m phase. N and the aliphatic core radius of quasi-spherical micelles R_ch are listed in the Table 5. ii) A body-centered cubic structure has been found by Gulik [11] and by Sakya [26] by freeze-fracture or by X-ray diffraction.

5.1.2 Q_m phase

The Q_m phase of space group Pm3n contains two types of discrete micellar aggregates: 2 in Wyckoff position "a" (0, 0, 0; 1/2, 1/2, 1/2) and 6 in Wyckoff position "c" (1/2, 1/4, 0) per unit cell, according to the International Table. Two alternative models of this phase have been proposed to take this into account. i) The model proposed by Fontell [27] assumes 8 identical prolate micelles per cell which rotate isotropically or anisotropically according to their sites "a" or "c" in the unit cell. ii) Charvolin and Sadoc [28] have proposed a structure of the Pm3n phase which contains two types of micelles; they assumed that each micelle in position "a" and in position "c" is contained in a different space limited by a dodecahedron and by a slightly distorded tetrakaidecahedron, respectively. Both polyhedra are shown in Figure 3a. From the cubic lattice parameter ($a = 10$ nm), the polyhedron edge, the dodecahedron volume and the tetrakaidecahedron volume were calculated to be 2.3 nm, 93 nm^3 and 139 nm^3, respectively. Thus, the volume of the tetrakaidecahedra is about 1.50-fold that of the dodecahedra and the volume of the micelles is assumed to be proportional to the volume of the host polyhedral cages. Charvolin and Sadoc suggested that the micelles in position "a" are spherical or spheroid whereas the larger anisotropic micelles in position "c" are disc-shaped aggregates (Fig. 3d). X-ray scattering studies and electron microscopic examination [11] have supported this view: the micelles in position "c" formed by gangliosides resembled oblate ellipsoids with an ellipticity of 0.66 [29,30]. We will use this model and these results for our following calculations and our discussions. According to this model, for a given concentration and lattice parameter a_{Q_m} of the cubic lattice, the volume fraction of the chain per cell and the volume of the cores of the micelles in positions "a" and "c" can be calculated giving the corresponding aggregation numbers N_a and N_c:

$$N_\mathrm{a} = C_\mathrm{v,ch}(a_{Q_\mathrm{m}})^3/(11V_\mathrm{ch}) = N_\mathrm{c}/1.5\,. \quad (5)$$

Table 6 lists the lattice parameters and the parameters of the aggregates for the concentrations $Ci_\mathrm{v,ch}$ corresponding to the appearance of the Q_m phase and the concentrations $Cf_\mathrm{v,ch}$ corresponding to the $Q_\mathrm{m} \Leftrightarrow H_\alpha$ transition

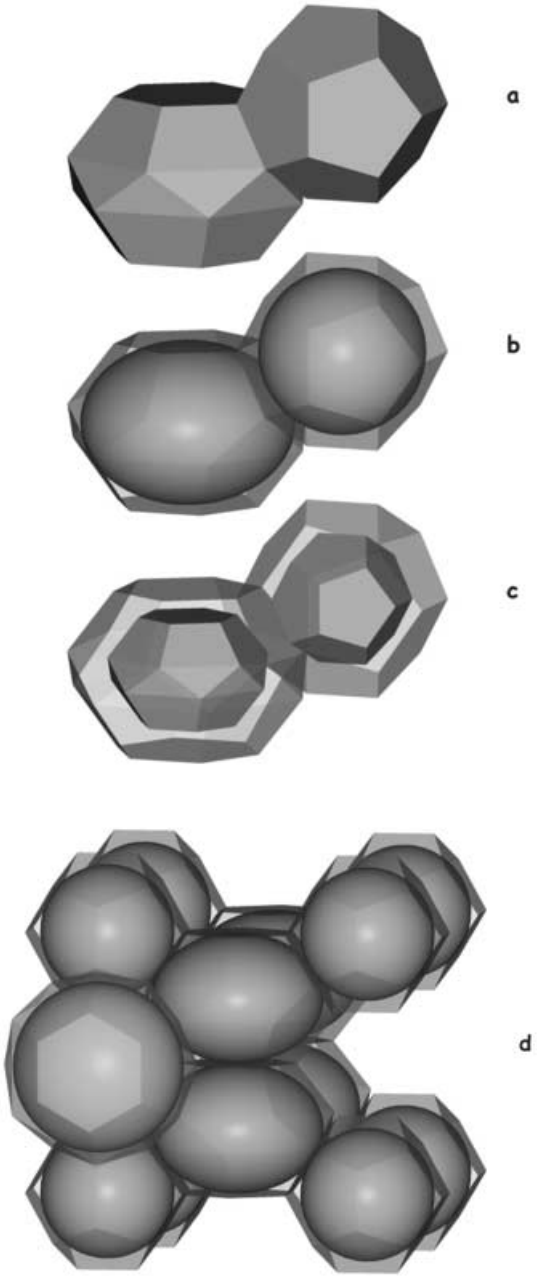

Fig. 3. a) Polyhedral representation of the cages. Dodecahedron and tetrakaidecahedron. b) Spherical micelle in a dodecahedron and disc-shaped micelle in a tetrakaidecahedron. In this figure the micelles are tangent to the polyhedral faces; in the text R^* is the radius of the spherical micelle tangent to the dodecahedron faces and a^* and b^* are the major and minor axes of the ellipsoidal micelle tangent to the tetrakaidecahedron faces. c) Polyhedral representation of the aggregates. The smaller polyhedra in the cages correspond to the aliphatic cores of the micelles (the actual shape of the core does not contain any corners but is of smooth geometry) which are surrounded by a hydrophilic part corresponding to the solvated head groups. d) Pm3n phase. Assembly of cages containing two types of micelles embedded in water according to the model of Sadoc and Charvolin [28].

for (αM), (Ac) and (L). These aggregate parameters are: i) N_a and $R_{ch,a} = (0.239\ N_a\ V_{par})^{1/3}$ the aliphatic core radius of quasi-spherical micelles in site "a"; ii) N_c and both axes a_{ch} and b_{ch} of the oblate ellipsoïd in site "c", $a_{ch} = (0.362\ N_c\ V_{par})^{1/3}$ and $b_{ch} = 0.66\ a_{ch}$, calculated with a core ellipticity of 0.66.

Recently, such a polyhedral representation of the reverse micellar aggregates in the Fd3m cubic phase has been studied in a phytanyl-chained glucolipid/water system [31].

5.2 Hexagonal phase

When the hexagonal phase is adjacent to the cubic phase Pm3n ((αM), (Ac) and (L)), the (10) peak of the hexagonal phase is in the continuity of the (211) peak of the cubic phase and the parameter of the hexagonal phase is $a_{H_\alpha} = (\sqrt{2}/3)\ a_{Q_m}$ at the respective phase boudaries. This epitaxial relationship which involves the (10) reticular planes of H_α transforming into the (211) reticular planes of a cubic phase has been observed in different systems [26, 32].

On the assumption of infinite cylinders with a circular cross-section, the radius of the core of cylindrical micelles R_{H_α} can be calculated as a function of concentrations and the lattice parameter:

$$R_{H_\alpha} = (\sqrt{3}/2\pi)^{1/2}\ a_{H_\alpha} (C_{v,ch})^{1/2}\,. \qquad (6)$$

The values of R_{H_α} are listed in Table 4. The radii of the aliphatic cores of cylinders increase with concentration to attain a value smaller than the expanded chain length and the areas per polar head slightly decrease. The H_α phase of (αM), (Ac), (L) and (B) was observed up to $C_m = 0.95$, their hydrated polar region length decreases from 1.0 nm to 0.55 nm, 1.1 nm–0.65 nm, 1.0 nm–0.6 nm and 1.6 nm–0.86 nm, respectively. In the H_α phase of (βM) the radius R_{H_α} is almost constant and the hydrated polar head region length decreases from 1.4 nm to 0.9 nm.

5.3 Intermediate phase

The H_α phase of (βM) turns into a centred rectangular phase M_α (cmm) by deformation of the cross-section of the cylinders.This deformation is incompatible with hexagonal symmetry [33]. The parameters of M_α depend on concentration and temperature: $a_{M_\alpha} = 9.75$ nm, $b_{M_\alpha} = 4.64$ nm at 20 °C and $C_m = 0.75$; $a_{M_\alpha} = 10.33$ nm, $b_{M_\alpha} = 4.78$ nm at 38 °C and $C_m = 0.83$.

5.4 Cubic phase (Ia3d)

This phase was observed over a narrow range of concentration and temperature on the phase diagrams, except for (βM). Its existence range is shown by the dotted line. Table 4 lists the lattice parameters of this phase.

The configuration of this phase, formed by two unconnected labyrinths of cylinders, has been described elsewhere [34]. Each junction involves three cylinders at angles of 120° parallel to direction [110]. The radii of the cylinders core, R_{Q_α}, can be calculated from the relationship in [34]:

$$C_{\mathrm{v,ch}}(a^3_{Q_\alpha}/24) = \pi R^2_{Q_\alpha}\, l_1(1 - 0.491\, R_{Q_\alpha}/l_1)\,, \qquad (7)$$

$$l_1 = a_{Q_\alpha}/\sqrt{8}\,. \qquad (8)$$

24 is the number of portions of the cylinder in the cubic cell, 0.491 is a coefficient which depends on the nature of the junction of the cylinders, and l_1 is the cylinder length (the distance between two neighbouring junctions in the same labyrinth). The surface area of each cylinder is obtained from the relationship

$$S = 2\pi R_{Q_\alpha}\, l_1(1 - 0.735\, R_{Q_\alpha}/l_1)\,. \qquad (9)$$

The surface area per polar head at the hydrophobic/hydrophilic interface σ is given by

$$\sigma = 24\, S\, V_{\mathrm{ch}}/(C_{\mathrm{v,ch}} a^3_{Q_\alpha})\,. \qquad (10)$$

The cylinder radii and the surface areas per polar head for the different compounds are listed in Table 4.

5.5 Lamellar phase

The L_α phase has not been observed *in situ* by X-ray diffraction below 95 °C, except for (βM). Its lattice parameter (4.0 nm) was slightly larger than that of the smectic phase on account of the polar hydration.

6 Discussion

The five compounds studied (αM), (βM), (L), (Ac) and (B) form thermotropic mesophases though the two anhydrous compounds (L) and (Ac) are non-crystalline solids. With water, they exhibit different lyotropic phase behaviours and all the curved phases which form are of type 1. Thus, the size and the type of linking affect the structure of the anhydrous compounds and the lyotropic phase formation, but not the formation of smectic phases.

6.1 Dry compounds

In the non-crystalline compound (Ac), the volume of the stretched chains of the molecule does not fill the space between the acetyl groups; the chains are melted or partially melted and disengaged. A voluminous linkage seems to prevent the formation of a lamellar crystalline order, but not the formation of a smectic phase at high temperature. Above 100 °C, the molecules are in a dynamic state and the hydrogen bonding that holds the polar head together often breaks and reforms; the smectic phase forms. On the other hand, although in the fucopyranoside, the equatorial CH_2OH group on C5 of the sugar ring is replaced by an equatorial CH_3 group, Sakya [35] shows that these compounds, insoluble in water at room temperature, remain crystalline up to 73 °C and do not exhibit thermotropic or lyotropic phases. Thus, a CH_3 group between the chain and the polar head would prevent the crystal formation, but a CH_3 group in the ring would prevent the smectic formation phase, for it affects the degree of intermolecular hydrogen bonding. It is more difficult to explain why the compound (L) is amorphous. We suggest that the lateral spacing between the aliphatic chains is increased by the attachment of the cyclic moiety to the branched acyclic chain. In some branched alkylglucosides studied by Nilsson [36], the neat surfactants also form an amorphous phase. In the same way, in a study of branched nonionic oligo-oxyethylene amphiphiles, Kratzat shows that in some dry compounds no crystallization is observed [37].

The non-crystalline state of (Ac) and (L) could also result from the lyophilized state that Vill [38] noticed with some glycosides. However (Ac), (L) and (B) have been lyophilized in the same way and the (B) molecules give an insoluble crystal at room temperature. In the last case, the additional carbonyl group close to the polar head is capable of hydrogen bonding and has a very high degree of polarizability [39] that leads to the Krafft temperature being higher than 40 °C. However, the amide group has a relativeley small dependence on the melting point; the discrepancy is only 12 °C between the melting temperatures of the crystals (αM) and (B) and it is 20 °C between the amorphous (L) and the crystal (B); this can be due to the non-crystalline state of (L).

6.2 Lyotropic phases: packing of discrete micelles and space-filling polyhedra

Four diagrams, (αM/water), (Ac/water), (L/water) and (B/water), are similar, but the diagram of (βM/water) is different. In the low surfactant concentration zone of each of the five diagrams, the main differences lie in the existence of ordered micellar phases. The three surfactants (αM), (Ac) and (L) form a cubic phase Q_{m} (space group Pm3n) over a wide composition and temperature range. The two surfactants (αM) and (Ac) form a body-centered cubic phase Q'_{m} (space group Im3m) at higher water content over a much narrower concentration and temperature range. At high surfactant concentrations and at a temperature higher than 100 °C, the first four binary systems exhibit a lamellar phase L_α in the continuity of the smectic phase and a very narrow cubic bicontinuous phase Q_α (space group Ia3d) which only occurs at about 90 °C (C_{m} about 0.9). These diagrams are essentially characterized by a hexagonal phase H_α over a very wide temperature and concentration range. H_α is observed with a few molecules of water per monomer. Consequently, a molecule with a bulky linkage (Ac), or a polarized linkage (B), or with a bend between the head and the tail (αM), preferentially builds curved interfaces with a packing parameter inferior or equal to 1/2; a wide, partially hydrated

Table 7. Number of molecules of water per molecule of surfactant at phase transitions.

Phase	Q'_{m} (Im3m)	Q_{m} (Pm3n)	H_α (p6m)	M_α (c.m.m.)	Q_α (Ia3d)	L_α
(Ac)	49	40 18	18 2		< 2	
(αM)	39	28 19	19 1.5		< 1.5	
(L)		26 10	10 1.5		< 1.5	
(B)			25 5		5	
(βM)			28 11	11 6	6 4	< 4

polar head with a weak charged linkage (L) produces the same effect.

In these sugar-based derivative/water mixtures, an amount of water (estimated to be about 10 molecules of water per molecule of surfactant) is necessary to solvate the polar heads because hydrogen bonding can occur to the polar head functional groups; the excess of water separates the aggregates as a continuous film. In our study, different phases are observed at high water content (40 molecules of water per monomer) or with a few molecules of water (less than 2 molecules of water per monomer) (Tab. 7). When the water content decreases the headgroup parts are solvated but the water film disappears, and at low water content ($<$ 10 molecules of water per monomer) there is no longer a free water layer between the micelles. It is suggested that different models of phase structure can be used to take this into account.

For both cubic phases (Im3m and Pm3n) the micellar model consists of disjoined aggregates separated by a continuous film of water. The body-centred cubic phase exists at high water content and its structure is modelled by a packing of identical "rigid" spheres embedded in water; for this cubic mode the closest packing of spheres takes place in the [1,1,1] array. The crystallographic data and chemical compositions of this phase are used to assess the dimensions of the micelles in the unit cubic cell. The radius of the the closely packed "rigid" spheres is $R_{\mathrm{s}} = (\sqrt{3}/4)a_{Q'_{\mathrm{m}}}$ and the radius of the aliphatic cores is $R_{\mathrm{ch}} = (0.239\ N\ V_{\mathrm{par}})^{1/3}$.

In contrast to the Im3m phase, the Pm3n phase which contains two types of micelles requires another kind of analysis. A plausible model would be an arrangement of discrete micelles in an assembly of two types of cages in order to pack the space completely. Thus, the structure of the Pm3n phase is described as being analogous to the packing of polyhedra in clathrate hydrates in terms of space-filling host polyhedra arranged in a cubic cell. This model requires the size of micelles to be consistent with the dimensions of polyhedra. At high water content the smaller aggregates in dodecahedra and the larger in tetradecahedra are assumed to be discrete micelles surrounded by a film of water. At lower water content the size of polyhedra, as well as the parameter of the unit cubic cell, decrease and each micelle surrounded by a water shell takes up the shape of its own cage; thus, the aggregates are faceted in the same way as the polyhedra faces when the film of water thins down. At still lower water content the polar heads are solvated but the water film no longer exists: the discrete spherical or oblate micelles are replaced by a polyhedral cell filled with a hydrophobic core surrounded by a hydrophilic part consisting of hydrated heads without free water molecules. Such a model proposed by Sakya [26] resembles the model of intermediate phases proposed by Hagslätt [33]. According to this cell model, it is energetically advantageous to maintain a constant thickness of the hydrophilic layer phase between the neighbouring cells. According to Turner [40], if, in an inverted lipid-water structure, hydrocarbon packing and bending energy are the two main terms of the free energy, the constant surface thickness minimizes the free packing energy when a constant mean curvature minimizes the bending energy and the structure arises from a compromise. In a model of a space-filling polyhedral cell containing an aliphatic core surrounded by a hydrophilic region (Pm3n, hexagonal or rectangular direct phases), the aliphatic cores are no longer spherical, oblate or cylindrical but the melted chains stack and fit the curvature of interfaces to maintain a constant thickness of the hydrophilic part between the neighbouring aggregates. The hydroxyls near the end of the sugar ring, but on the outside, form strong hydrogen bonds to the opposite interfaces and this inter and intra molecular hydrogen bonding with water stabilizes the phase. This model is suited to molecules with bulky polar heads and which form an extensive hydrogen-bonded network at low water content. From a model of the assemblies of filling polyhedra, both Im3m and Fm3m phases have been also visualized as a packing of truncated octahedra and rhombic dodecahedra, respectively, and Luzzati has described their relationship to non-congruent infinite periodic minimal surfaces [41].

The direct hexagonal phase consists of infinite cylinders of amphiphiles that are packed with a hexagonal symmetry in an aqueous medium. Another cell topology can be defined by the axes of the hydrophobic cylindrical cores forming a hexagonal array of lines (called the skeleton) and a surface (called the frame) [42], which divides the aqueous space symmetrically. At low content of water (less than 10 molecules per monomer) when the water film thins down, the cylinders are replaced by hexagonal prisms parallel to the sides of the cell; these structural elements pack to form a honeycomb lattice that separates the aggregates and maintains a constant thickness of the opposite hydrophilic layers.

The bicontinuous cubic phase Ia3d is visualized by a model of rods or as an infinite periodic minimal surface or I.P.M.S. (Schœn's G surface) which divides the water layer symmetrically. The film of water is assumed to be of constant thickness. In our study this cubic phase appears

at high temperature and exists with a few molecules of water, thus, the midsurface associated to the I.P.M.S. divides opposite hydrophilic layers symmetrically.

6.2.1 Behaviour of the (αM/water), (Ac/water) and (L/water) systems

The structure of the molecules (αM) and (Ac) favors a spherical curvature of micelles from the c.m.c. up to about 30 molecules of water per monomer which allows quasi-spherical micelles to form and a micellar ordered phase (Im3m) to occur when the solutions contain about 45 molecules of water per molecule of surfactant (Tab. 7). According to the model of a packing of rigid spheres in a body-centred mode of space group Im3m, the radii of the micelles R_s are 2.77 nm for (αM) and 2.86 nm for (Ac) and the radii of the aliphatic cores R_{ch} are 1.84 nm for (αM) and 1.80 for (Ac), (Tab. 5). These parameters are identical for the micelles in a diluted solution. Thus, the shape and the dimension of the micelles in the cubic phase Im3m are similar to those found in the micellar solutions and assumed to be quasi-spherical. These calculated values suggest that the micelle mesostructure in the body-centred cubic phase is inherited from the parent micellar phase I_α. The smaller thickness of the hydrated polar heads together with the water layer ($R_s - R_{ch}$) is about 1 nm, which is consistent with a hydrated polar head region length containing about 10 molecules of water per head surrounded by a film of water. However, the radius of the apolar core of the micelles, assumed to be spherical, turns out to be longer than the expanded chain length with 12 carbon atoms ($l_m = 1.65$ nm according to Tanford [20]), (in this last case the difference ($R_{ch} - l_m$) was less than 10%). If we compare this result with different data reported in the literature, this discrepancy was comparable or smaller [26, 41]. According to Luzzati, the inequality $R_{ch} < l_m$ proceeds from the value of R_{ch} which is calculated from a model which strictly partitions the apolar and polar moieties of the molecules. To elude the anomaly $R_{ch} > l_m$, Luzzati [41] has introduced the idea of a different partition, where the polar head group comes into contact with the paraffinic core of the micelles. Thus, the $R_{ch} < l_m$ ceases to be a packing constraint.

The cubic phase Q_m(Pm3n) of (Ac) and (αM) is adjacent to the cubic phase Q'_m (Im3m) at $T < 40\,^\circ$C and at lower water content. At the transition the water content of the system corresponds to 40 molecules of water per monomer for (Ac) and 28 for (αM), (Tab. 7). With 8 micelles in the Q_m unit cell and 2 micelles in the Q'_m unit cell, the lattice parameters, a_{Q_m} and $a_{Q'_m}$, should be in a ratio of $(8/2)^{1/3} = 1.587$, at the transition $Q'_m \leftrightarrow Q_m$, if the number of micelles per unit volume is the same for both phases. For (αM) and (Ac) the ratios are 1.62 and 1.65, respectively. This result suggests that a new ordered micellar phase occurs without fusion events at the transition. The new structure is a packing of two types of discrete micelles in a water matrix; according to this model, the calculated aggregation number of the smaller micelles in the dodecahedra and the "rigid" spheres in the Im3m phase are similar (Tabs. 5 and 6). This relationship between both neighbouring phases suggests that the quasi-spherical micelles which are centered at positions "a" are inherited from the Im3m parent phase. If we assume that the quasi-spherical micelles are contained in dodecahedra, their maximum radius R_{sd}* is the radius of the inner sphere tangent to the faces of these polyhedra (Fig. 3b). On the other hand, the micelles in the tetrakaidecahedra are anisotropic in shape and can be modelled by an oblate ellipsoid. This model is consistent with the freeze-fracture electron microscopy patterns because the ellipticity of the larger disc-shaped aggregate contained in these polyhedra is also $b^*/a^* = 0.77$ (Fig. 3b). (In our model we have taken 0.66 for the ellipticity of the aliphatic core disc according to the electron microscopy data). Thus, the Im3m $\leftrightarrow$ Pm3n transition corresponds to a rearrangement and a slight deformation of the micelles of the body-centred cubic phase. The calculated dimensions of the micelles in the Pm3n phase are listed in Table 8. When the Pm3n phase is formed with about 30 molecules of water per monomer, the discrete micelle parameters are consistent with the size and the shape of polyedra. Their radius R_{sd}, calculated with a hydration ratio of 10 molecules per monomer is $R_{sd} < R_{sd}$*. When the water content decreases the lattice parameter and the volume of polyhedra decrease and the aggregation number of the micelles increases (with (Ac) especially) so that, at the transition Pm3n $\leftrightarrow H_\alpha$, the micelles are tangent to the polyhedral faces (Tab. 8 and Fig. 3b). The core dimension of the spherical micelles becomes $R_{ch} = 1.90$ nm for (Ac) and $R_{ch} = 1.82$ nm for (αM); thus, the discrepancy with the expanded chain length increases up to 15% with (Ac) and the assumption of the quasi-spherical micelles in site "a" is no longer consistent; moreover it is difficult to know how the dimensions of the disc-shaped micelles change. At the transition Im3m $\leftrightarrow$ Pm3n, a micellar interpretation is justified (Fig. 3d). When the water content decreases up to the transition Pm3n $\leftrightarrow H_\alpha$ which takes place with about 20 molecules of water per monomer, the water film thickness becomes very weak and the formation of faceted aggregates is suggested just before this transition.

In contrast to (αM) and (Ac), the linkage of the (L) molecule is weakly charged and from the c.m.c. disk-shaped anisotropic aggregates are formed; their mean curvature is smaller than that of micelles obtained with (αM) and (Ac). These deformed micelles cannot give the Im3m micellar cubic phase. However, the formation of the Pm3n micellar cubic phase is possible in a large range both in temperature and concentration. At the transition (micellar phase $\leftrightarrow$ Pm3n) the aggregation numbers of the micelles in the I_α solution and in the dodecahedra of the Pm3n phase are similar. If we assume that these micelles are spherical in the cubic phase, then they are tangent to the polyhedral faces and their aliphatic cores have a radius of $R_{ch} = 1.92$ nm which exceeds the fully extended length l_m of the chain. According to Luzzati [41], a portion of the head groups can be embedded in the chains; in this case R_{ch} can be much larger than l_m. The value of the radius R_{ch} increases with the concentration up to $R_{ch} = 1.99$ nm; the discrepancy with the extended chain length becomes

Table 8. Parameters of micelles encased in two types of cells. R_s: radii of micelles assumed to be spherical; a and b major and minor axes of micelles assumed to be oblate; indexes i and f are used at onset of Q_m and at $Q_m \Leftrightarrow H_\alpha$ transition, respectively. "*" corresponds to the maximum values of the parameters when discrete micelles are tangent to the polyhedral faces.

Cells	Dodecahedra		Tetrakaidecahedra				Dodecahedra		Tetrakaidecahedra			
Micelle parameters	R_{sd}* (nm)	R_{sd} (nm)	a_i* (nm)	a_i (nm)	b_i* (nm)	b_i (nm)	R_{sd}* (nm)	R_{sd} (nm)	a_f* (nm)	a_f (nm)	b_f* (nm)	b_f (nm)
(αM)	2.65	2.50	3.40	3.05	2.60	2.25	2.55	2.57	3.25	3.15	2.50	2.33
(L)	2.80	2.70	3.57	3.30	2.75	2.44	2.52	2.74	3.23	3.36	2.47	2.48

substantial and suggests (as in the diluted micellar solutions) a deviation from perfectly spherical micelles to anisotropic aggregates, which implies a dynamic disorder of the micelles centered at position "a". Therefore, we assume that the aggregates modelled as polyhedra form as soon as the transition micellar phase $\leftrightarrow$ Pm3n is reached. At the transition Pm3n $\leftrightarrow H_\alpha$ the disjoined micelle parameters are inconsistent with the size of cages (Tab. 8), the volumes of aggregates are equal to that of polyhedra which represent the shape of the aggregates (Fig. 3c) and there are about 6 packed molecules per polyedral face. The actual shape of aggregates does not contain any steep corners but is of smooth geometry. However this model implies that the aggregate dimension changes in different directions and the aliphatic cores are not necessarily perfectly spherical or oblate. The boundaries between the cells are weakly charged; the Coulomb interactions vary little with temperature and thus the Pm3n phase is located in a wide range of temperatures ($T < 90\,^\circ$C) and a concentration domain limited by two vertical lines. In contrast to (L), for (αM) and (Ac) the Pm3n phase exists in a narrower domain for both temperature ($T < 45\,^\circ$C) and concentration.

The analogy of the space-filling polyhedra representation with foams has been pointed out by Luzzati [41]. In the Pm3n phase Plateau's conditions are fulfilled and the system behaves as a dry foam especially if the thickness of the interstitial layer between the micelles is negligible. According to Weaire and Pheland, the lowest surface energy seems to correspond to this structure [43].The analogy with foams means that the polar heads should be highly hydrated; it is the case for (αM) and (Ac) at water concentrations lower than about 25 water molecules per monomer and particularly for (L) at 10 molecules of water per monomer. At higher water content this structure falls short of fulfilling Plateau's conditions and for (Ac) and (αM) the Pm3n phase turns into the Im3m phase. The sequence Im3m $\leftrightarrow$ Pm3n as a function of the water content decrease is consistent with the theoretical expectations and experimental results reported in the literature.

In the phase diagram, the phase H_α is located in a region which is limited by phase boundaries which are practically parallel to the temperature axis and it spans a wide range of both temperature and concentration. This phase is adjacent to the Pm3n and appears at a water content corresponding to about 20 molecules of water per monomer of (Ac) and (αM) and 10 molecules of water per monomer of (L), (Tab. 7). By increasing the surfactant concentration the changes of a_{H_α} are weak (Tab. 4); the radius of the aliphatic circular cylinders increases from 1.3 nm to about 1.5 nm (which is less than the expanded chain length) for (Ac) and (αM) (this value increases from 1.43 nm to 1.61 nm for L). The length of the hydrated polar head decreases from 1.1 nm to about 0.6 nm which is inconsistent with the polar head size. For a range of compositions at low hydrations (less than 10 molecules of water per monomer) a cage model is more realistic than a long circular rod model.

Like the phase H_α, the bicontinuous cubic phase Q_α (Ia3d) exists with a very low content of water, the areas per polar head are comparable to those found for cylinders of the hexagonal phase and the transition $H_\alpha \leftrightarrow Q_\alpha$ is thermotropic.

6.2.2 Behaviour of the (B/water) system

In contrast to (αM) (Ac) and (L), the Kraft line is observed in the phase diagram of the (B)/water system. The molecules of (B) with an amide linkage give slightly more anisotropic micelles than (L) and the micellization occurs at a temperature above 45 °C. This slightly different shape of aggregates and the temperature effect suppress the appearance of micellar ordered phases and induce the hexagonal phase directly from the elongated micelles. At first, this phase is described as long cylinders that are packed with a hexagonal symmetry and is characterized by a strong variation of its parameter with the water content decreasing (Tab. 4). Then the parameter changes very slowly, the radius of the aliphatic core is larger than the expanded chain length and a cage model seems better. As for the three previous systems the transition from the H_α phase to the Q_α phase is thermotropic.

6.2.3 Behaviour of the (βM/water) system

The binary diagram of the (βM)/water system is very different. Among the five surfactants studied, the micelles of (βM) with an aggregate number of 132 above the c.m.c. are the most anisotropic micelles, the micellar cubic phases do not occur and the H_α phase is found adjacent to the micellar phase I_α. Moreover, (βM) exhibits an intermediate phase $M_\alpha$between H_α and Q_α. The transitions $M_\alpha \leftrightarrow Q_\alpha \leftrightarrow L_\alpha$ are mainly thermotropic, the change of curvature is produced by temperature, on heating the chains become more flexible, the bonds between the hydroxyl groups are modified and the amplitude of vibrations increases.

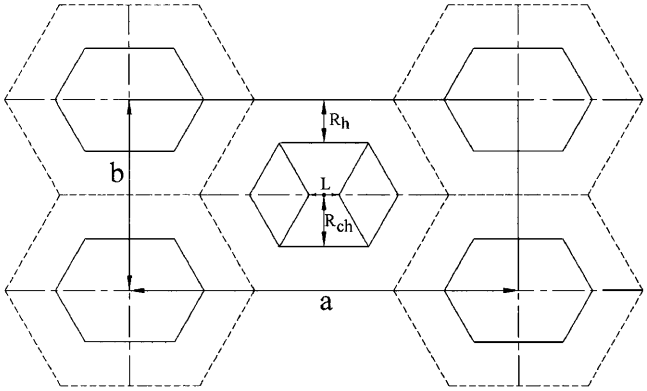

Fig. 4. Centred rectangular phase M_α in the β maltoside/water system. Model of cell according to reference [33].

The intermediate ribbon phase M_α is commonly described by elongated rods with a non-circular section that packs on a deformed hexagonal two-dimensional lattice. A cellular model has also been advanced [33] to describe the M_α phase formed by ionic surfactants: the aggregate and the cell are modelled by a deformed hexagon and the water layer separating the two aliphatic interfaces is constant. The stability is assumed to derive from the electrical repulsions between charged opposed interfaces. It was also demonstrated that the centered rectangular symmetry was the most energetically favoured cell. Previously a similar cell model approach has been used to describe the structure of cubic and hexagonal phases especially at low water content. The intermediate phase appears with 11 molecules of water per monomer of (βM) (Tab. 7) and a cell model has been retained. Figure 4 shows a lattice of centred rectangular phase (cmm) based on the model described in [33]. The dimensions of the aliphatic core are $L = 0.5$ nm and $R_{\rm ch} = 1.43$ nm, where L is the length of the lamellar-like part of the aggregate and $R_{\rm ch}$ the smallest dimension of the aliphatic part; the hydrated polar heads completely fill the space containing the 1.0 nm thick hydrophilic region and there is no free water between the neighbouring aggregates. The M_α phase is not electrically stabilized as compared with ionic surfactants but its formation can be due to inter and intra molecular hydrogen bonds. However, the deformation of the cylinder cross-section is not strong enough to prevent the occurrence of the Ia3d phase as was reported in the SDS/water system [44]. In contrast to the cubic phases, hexagonal phases or lamellar phases, the parameters a and b of the centred rectangular phase increase with an increase of the surfactant and temperature. This difference presumably derives from the different types of inter and intra molecular interactions of the head groups with the solvent.

To our knowledge, this intermediate phase M_α has only been observed with ionic surfactants in water and never in non-aqueous polar solvents or non-ionic surfactants. Its presence in the (βM)/water diagram shows the peculiar behaviour of this surfactant which presents some properties similar to the ionic surfactants.

The different properties of the dry (αM) and (βM) and their behaviour in water is difficult to explain. An explanation can be suggested from the flexibility of the molecule of (βM); by free rotation it turns till the sugar rings are opposed [45] and, from this outline, intramolecular bonds can be formed. When the surfactant fraction is about 0.75, the thickness of the water layer becomes negligible and the cage model is more realistic. When the temperature increases the molecular vibrations are more important and the two-dimensional M_α phase turns into a Ia3d bicontinuous cubic phase. The hydration of the polar head of (βM) is more dependent on the temperature than the hydration of the polar heads of the other compounds studied. The molecule of (αM) is less flexible, therefore, the self-assembling is similar to that of (Ac) in water because the intermolecular bonds are similar.

7 Comparisons of the lyotropic behaviour of other non-ionic surfactants

Although the liquid-solid crystal behaviour of a variety of different sugar-derived molecules has been studied, relatively few binary diagrams have been published. The micellization of some disaccharides has been studied [16–18, 22] and the formation of some lyotropic phases has been reported [12, 22]. Recently, a study of the N-hexadecyl D maltoside/water system presents evidence for vesicle-type aggregate formation. In contrast, the formation of micellar aggregates from aqueous suspensions of N-hexadecyl-1 desoxylactitol is observed at 20 °C [46]. The "fixed" or "fluxional" head group structure is the important determinant of the aggregate nature; the acyclic open-chain part is amenable to wide conformational variations; a greater flexibility and a weaker head group association allow an easier interfacial curvature and a packing parameter change with concentration. Thus, a classical sequence of ordered phases could be observed with the N-hexadecyl-1 desoxylactitol.

In this study, the previous binary diagrams can be compared to the binary diagrams of gangliosides (GM1) [11], monosaccharides [5, 35, 47], linear or branched polyoxyethylene surfactants with an alkylchain of 12 carbons [26, 37, 48]. When the micelles remain spherical and small in the whole range of concentration, cubic micellar phases are observed: $Q'_{\rm m}$, $Q_{\rm m}$ and sometimes a face-centred cubic phase. This last phase forms when the ratio $V_{\rm h}/V_{\rm m}$ is higher than 0.5; $V_{\rm h}/V_{\rm m} = 0.68$ (C12E012) [26] and 0.71 (ganglioside GMIC [11]). However this ratio is not the single criterion for the existence of ordered micellar phases as the molecules of (αM) and (βM) have the same $V_{\rm h}/V_{\rm m}$ and (βM) does not even form a Pm3n phase. An H_α phase within such a large range of temperature and concentration is not observed in the binary diagrams of other non-ionic surfactants such as polyoxyethylene surfactants.

Binary technical alkyl polyglycoside/water systems have been intensively studied ($C_{8/10}$, $C_{10/12}$ and $C_{12/14}$) [49, 50]. The average degree of polymerisation (from 1.1 to

1.8) and the chain length distribution are responsible for the extent of the two-phase region. When the chain contains 12 carbon atoms the binary diagrams are complex and the cubic phase Q_α or micellar ordered phases are not observed.

The monosaccharides studied by Sakya [35] and Hall [51] do not exhibit hexagonal phases as broad as those observed with disaccharides such as (αM), (Ac), (L) and (B); however, the L_α and Q_α phases are present in a broader range. The ability to form a hydrogen-bonded network between molecules decreases with monosaccharides.

The hydration of the sugar ring is less dependent on the temperature than that of the polyoxyethylene [5]; the cloud point phenomenon is not observed with pure compounds and the micellar range is very broad in temperature and concentration.

8 Conclusion

This study of the thermotropic and lyotropic liquid crystalline behaviour of five amphiphilic disaccharide derivatives with an aliphatic chain of 12 carbons shows a progressive modification of self-association properties in water.

The lyotropic phase behaviour is affected not only by the ionic or rod-like nature of the molecule but also by the type of linking between two moieties of the molecule. This is particularly noticeable for the (αM) and (βM), where the difference only lies in the axial or equatorial orientation between the chain and the sugar rings. The disaccharide molecules bearing either two cyclic rings or one cyclic ring and an acyclic open-chain form exhibit a similar behaviour in water when their chain contains 12 carbon atoms. These surfactants in aqueous solutions can generate varying direct phases from a hexagonal (or a cubic phase of space group Ia3d at high temperature) to a micellar solution, on account of a suitable hydrophilic/hydrophobic balance of their molecules. The phases are not observed with an alkyl chain containing less than 12 carbon atoms [12] and the behaviour of the solutions is different with a chain of 16 carbon atoms [46]. With two sugar residues, the chemical structure of the head group has some effects on the spontaneous curvature of the aggregates: two different micellar ordered phases are observed if the micelles remain quasi-spherical when the surfactant concentration increases, as for (αM), (Ac) and (L) for instance. Hato has shown the effects of oligosaccharide stereochemistry with different head group conformations and particularly with increasing the sugar residue number [10].

The hydration of the polar heads and the ability to give rise to hydrogen bonding with neighbouring molecules leads to the lack of a film of free water between the interfaces as soon as the water content is less than 20 molecules per molecule of surfactant. A strong hydrogen-bonded network forms between the opposing interfaces; the cage model is suggested to explain the very large range of the hexagonal phase which can exist with only a few water molecules per monomer.

The authors thank F. Bostel for assistance in solving instrumentation problems and D. Moscato for useful comments.

References

1. R. Garelli-Calvet, F. Brisset, I Rico, A. Lattes, Synth. Commun. **23**, 35 (1993) and cited references.
2. a) T.J. Williams, N.R. Plessas, I.J. Goldstein, Arch. Biochem. Biophys. **195**, 145 (1979); b) D. Abran, F. Boucker, T. Hamanaka, K. Hiraki, Y. Kito, K. Koyama, R. Leblanc, M. Machida, G. Munger, R.M. Seidou, M.J. Tessier, Colloid Interface Sci. **128**, 230 (1989); c) D. Plusquellec, G. Chevalier, R. Talibart, H. Wroblewski. Ann. Biochem. **179**, 145 (1989); d) R. Garelli, R. Calvet, P. Latge, I. Rico, A. Lattes, A. Puget, Biochim. Biophys. Acta **1109**, 55 (1992) and cited references.
3. a) J.S. Lazo, D.E. Quinn, Anal. Biochem. **102**, 68 (1980); b) F. Brisset, R. Garelli-Calvet, J. Azema, C. Chebli, I. Rico-Lattes, A. Lattes, A. Moisand, New J. Chem. **20**, 595 (1996).
4. H. Koch, R. Reck, H. Röper, Inf. Chim. **347**, 78 (1993).
5. a) K. Shinoda, M. Fukuda, A. Carlsson, Langmuir **6**, 334 (1990); b) K. Shinoda, A. Carlsson, B. Lindman, Adv. Colloid Interface Sci. **64**, 253 (1996).
6. a) F. Nilsson, INFORM **7**, 490 (1996); b) F. Kiraly, R. Börner, G.H. Findenagg, Langmuir **13**, 3308 (1997).
7. F. Nilsson, O. Söderman, I. Johansson, Langmuir **12**, 902 (1996).
8. P. Boullanger, Y. Chevalier, Langmuir **12**, 1771 (1996).
9. X. Auvray, B. Labulle, C. Petipas, J.N. Bertho, T. Benvegnu, D.J. Plusquellec, Mater. Chem. **7**, 1373 (1997).
10. M. Hato, H. Minamikawa, Langmuir **12**, 1658 (1996).
11. A. Gulik, H. Delacroix, G. Kirschner, V. Luzzati, J. Phys. II **5**, 445 (1995).
12. X. Auvray, C. Petipas, R. Anthore, I. Rico-Lattes, A. Lattes, Langmuir **11**, 433 (1995).
13. P. Sakya, J.M. Seddon, R.H. Templer, J. Phys. II **4**, 1311 (1994).
14. a) T. Haneman, E. Schumacher, W. Haase, F. Lichtenthaler, Liq. Cryst. **22**, 47 (1997). b) B. Pfannemuller, W. Welte, Chem. Phys. Lipids **37**, 227 (1985).
15. F. Coste, M. El Ghoul, I. Rico-Lattes, A. Lattes, Langmuir **11**, 3644 (1995).
16. C. Dupuy, X. Auvray, C. Petipas, I. Rico-Lattes, A. Lattes, Langmuir **13**, 3965 (1997).
17. C. Dupuy, X. Auvray, C. Petipas, R. Anthore, F. Costes, I. Rico-Lattes, A. Lattes, Langmuir **12**, 3162 (1996).
18. C. Dupuy, X. Auvray, C. Petipas, R. Anthore, I. Rico-Lattes, A. Lattes, Langmuir **14**, 91 (1998).
19. P. Latge, I. Rico, L. Garelli, A. Lattes, J. Dispersion Sci. Technol. **12**, 227 (1991).
20. C. Tanford, *The Hydrophobic Effect: Formation of Micelles and Biological Membranes* (Wiley Interscience, New York, 1973).
21. a) M.A. Marcus, Mol. Cryst. Liq. Cryst. Lett. **3**, 85 (1986); b) B. Pfannemuller, W. Welte, E. Chin, J.W. Goodby, Liq. Cryst. **1**, 357 (1986).
22. a) M.A. Marcus, P.L. Finn, Liq. Cryst. **3**, 381 (1988); b) G. Warr, C. Drummond, F. Grieser, B. Ninham, D. Evans, J. Phys. Chem. **90**, 4581 (1986); c) C. Cecutti, B. Focher, B. Perly, T. Zemb, Langmuir **7**, 2580 (1991).

23. Israelachvili, D.J. Mitchell, B.W. Ninham, J. Chem. Soc., Faraday Trans. II **72**, 1425 (1976).
24. S.T. Hyde, J. Phys. C **7**, 209 (1990).
25. a) J.F. Sadoc, J. Charvolin, J. Phys. **47**, 683 (1986); b) J. Charvolin, J.F. Sadoc, J. Phys. Chem. **92**, 5787 (1988); J. Phys. **48**, 1559 (1987); c) J. Charvolin, J.F. Sadoc, Physica A **176**, 138 (1990).
26. P. Sakya, J.M. Seddon, R.H. Templer, R.J. Mirkin, G.J.T. Tiddy, Langmuir **13**, 3706 (1997).
27. K. Fontell, Colloid Polym. Sci. **268**, 264 (1990).
28. J. Charvolin, J.F. Sadoc, J. Phys. **49**, 521 (1988).
29. R. Vargas, P. Mariani, A. Gulik, V. Luzzati, H. Delacroix, J. Mol. Biol. **225**, 177 (1992).
30. V. Luzzati, R. Vargas, P. Mariani, A. Gulik, H. Delacroix, J. Mol. Biol. **229**, 540 (1993).
31. H. Minamikawa, M. Hato, Langmuir **14**, 4503 (1998)
32. V. Luzzati, J. Phys. II **5**, 1649 (1995).
33. H. Hagslätt, O. Söderman, B. Jönsson, Liq. Cryst. **12**, 667 (1992); **17**, 157 (1994).
34. A. Gulik, V. Luzzati, M. De Rosa, A. Gambacorta, J. Mol. Biol. **182**, 131 (1985).
35. P. Sakya, J.M. Seddon, V. Vill, Liq. Cryst. **23**, 409 (1997).
36. F. Nilsson, O. Soderman, I. Johansson, Langmuir **13**, 3345 (1997).
37. K. Kratzat, H. Finkelmann, Liq. Cryst. **13**, 691 (1993).
38. V. Vill, T. Böcker, J. Thiem, F. Fischer, Liq. Cryst. **6**, 349 (1989).
39. F. Ewing, J.W. Goodby, J.A. Haley, S.M. Kelly, P. Letellier, G. Mackenzie, Liq. Cryst. **23**, 759 (1997).
40. D. Turner, Z.-G. Wang, S. Gruner, D. Mannock, R. McElhaney, J. Phys. II **2**, 2039 (1992).
41. V. Luzzati, H. Delacroix, A. Gulik, J. Phys II **6**, 405 (1996).
42. P. Duesing, R. Templer, J. Sedon, Langmuir **13**, 351, (1997).
43. D. Weaire, Phil. Mag. Lett. **69**, 99 (1994); D. Weaire, R. Phelan, Phil. Mag. Lett. **69**, 107 (1994).
44. X. Auvray, T. Perche, R. Anthore, C. Petipas, I. Rico, A. Lattes, Langmuir **7**, 212 (1991).
45. C. Dupuy, Thesis, University of Rouen, 2001.
46. S. Bhattacharya, G. Acharya, Langmuir **16**, 87 (2000).
47. E. Smits, J. Engberts, R. Kellog, Liq. Crist. **23**, 481 (1997).
48. D.J. Mitchell, G.J.T. Tiddy, L. Waring, T. Bostock, M.P. McDonald, J. Chem. Soc. Faraday Trans-1 **79**, 975 (1983).
49. D. Nickel, T. Foster, W. von Ribinsky in *Alkyl Polyglycosides*, edited by K. Hill, W. von Rybinsky, G. Stall (VCH, Weinheim, 1997).
50. D. Balzer, Langmuir **9**, 3375 (1993).
51. C. Hall, G.J.T. Tiddy, B. Pfannemuller, Liq. Cryst. **9**, 527 (1991).